A new type of X-ray pulsar

Lidia M. Oskinova[1*], Yael Nazé[2], Helge Todt[1],
David P. Huenemoerder[3], Richard Ignace[4],
Swetlana Hubrig[5], Wolf-Rainer Hamann[1]

[1]Institute of Physics and Astronomy, University of Potsdam, 14476 Potsdam, Germany

[2]FNRS/Univ. of Liège, Dept A.G.O. (GAPHE), 4000-Liège, Belgium

[3] Massachusetts Institute of Technology, Kavli Institute for Astrophysics and Space Research,
70 Vassar St., Cambridge, MA 02139, USA

[4] Department of Physics and Astronomy, East Tennessee State University,
Johnson City, TN 37663, USA

[5] Leibniz Institute for Astrophysics Potsdam (AIP), An der Sternwarte 16
14482 Potsdam, Germany

[*]To whom correspondence should be addressed; E-mail: lida@astro.physik.uni-potsdam.de

Abstract

X-ray emission from stars much more massive than the Sun was discovered only 35 years ago. Such stars drive fast stellar winds where shocks can develop, and it is commonly assumed that the X-rays emerge from the shock-heated plasma. Many massive stars additionally pulsate. However, hitherto it was neither theoretically predicted nor observed that these pulsations would affect their X-ray emission. Here we report the discovery of pulsating X-rays from the massive B-type star ξ^1 CMa. This star is a variable of β Cep type and has a strong magnetic field. Our observations with the *XMM-Newton* telescope reveal X-ray pulsations with the same period as the fundamental stellar pulsation. This discovery challenges our understanding of stellar winds from massive stars, their X-ray emission, and their magnetism.

1   Introduction

Massive stars $(M_{\mathrm{initial}} \gtrsim 8 M_\odot)$ are among the key players in the cosmic evolution. These hot stars generate most of the ultraviolet radiation of galaxies and power their infrared luminosities.

Massive stars, their winds and their final explosions as supernovae provide significant input of radiative and mechanical energy into the interstellar medium, inject nuclear processed material, and largely drive the evolution of star clusters and galaxies.

The majority of all massive stars are of spectral type B. Stars with spectral subtypes B0-B2 are born with masses between $8\,M_\odot$ and $18\,M_\odot$. They are hot, with effective temperatures $T_{\mathrm{eff}} > 15\,000\,\mathrm{K}$. While still young and burning hydrogen in their cores, these stars oscillate with periods of a few hours [1]. The physical mechanism that drives these oscillations is well understood and is attributed to changes in the opacity within the star during the pulsation cycle ("κ-mechanism") [2]. A whole class of such variables is termed after its prototype β Cephei. A B0-B2 type star ends its life with a supernova explosion, when the stellar core collapses and leaves a neutron star as a remnant [3]. Fast rotating, strongly magnetic neutron stars may manifest themselves as radio and X-ray pulsars.

All hot massive stars drive stellar winds by their intense radiation. Photons that are scattered or absorbed in spectral lines transfer their momentum and thus accelerate the matter to highly supersonic velocities, typically of the order of $1000\,\mathrm{km\,s^{-1}}$. This driving mechanism is unstable [4]. It is generally believed that the wind instability may result in wind shocks where part of the wind material is heated to X-ray emitting temperatures. These wind shocks are often invoked to explain the X-ray emission which is ubiquitously observed from massive stars [5].

Typically, the observed X-ray spectra of single massive stars are thermal. In high-resolution, X-ray spectra are dominated by slightly blue-shifted and broad emission lines [6]. These line shapes can be explained as originating in a rapidly expanding stellar wind, consisting of hot X-ray emitting matter permeated with cool matter which attenuates the X-ray field [7, 8, 9].

A small fraction of massive stars, including some B-type stars, possess strong, large-scale magnetic fields [11, 12]. According to one hypothesis, such stars may have undergone a recent merger process which powered a dynamo mechanism [13, 14].
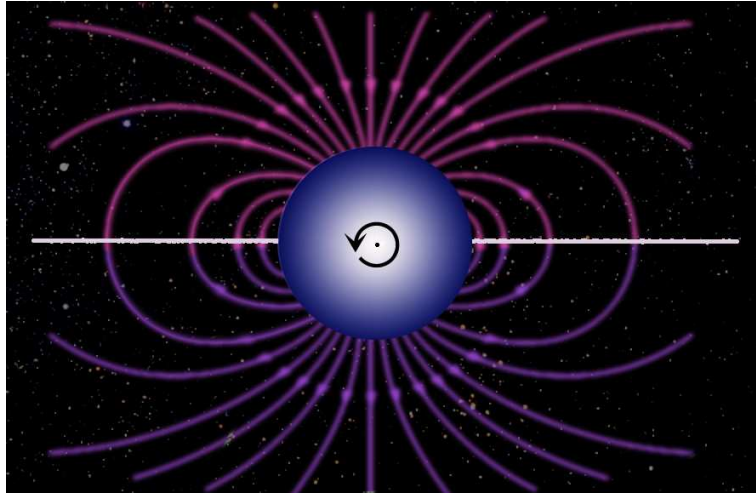
Figure 1: Sketch of the rotational and magnetic geometry for ξ^1 CMa. From the Earth the star is viewed nearly rotational pole-on (black dot). The star is a magnetic oblique rotator: its magnetic and rotational axes are inclined to each other by $\approx 79°$ [10]. Hence the magnetic equator (white line) is always seen nearly edge-on. The curved lines illustrate the dipole magnetic field geometry.

Strong magnetic fields can significantly influence the dynamics of stellar winds [15]. If the magnetic field has a dipole configuration, the strong field can in effect "channel" the wind toward the magnetic equator, where the wind streams from the opposite hemispheres collide. The formation of a strong stationary shock is predicted, and it is expected that the X-ray properties of stars with strong magnetic fields will be different from those of non-magnetic stars, e.g. the X-ray temperatures for magnetically confined winds should be are higher [16].

Fluctuations of the X-ray flux on rotational time-scale are reported for single massive stars (magnetic as well as non-magnetic) [17, 18], and may be related to large scale structures in the winds corotating with the star [19, 20].

The two models briefly outlined above (embedded wind shocks for non-magnetic objects and magnetically confined winds) are widely adopted to interpret the X-ray emission from single hot massive stars [21]. However, neither of these models accounts for the effects of stellar pulsations.

3

Table 1: Parameters of ξ^1 CMa

Distance	424 pc
Sp. Type	B0.5-B1IV
T_{eff}	27 000 — 28 000K
$\log L/L_\odot$	4.5
$R/R_\odot$	7 ± 1
Rotational velocity $v \sin i$	9 ± 2 km s^{-1}
Mass-loss rate $\dot{M}$	$< 10^{-10} M_\odot$ yr^{-1}
Wind velocity v_∞	~ 700 km s^{-1}
Polar magnetic field strength B_{p}	5 ± 1 kG
Pulsation period	0.2096 d
L_{X}	3×10^{31} erg s^{-1}

Parameters compiled from the literature, see text for details

The β Cep-type variable ξ^1 CMa, spectral type B0.5-B1 V-IV [22], is an ideal target to study the interactions between stellar pulsations, magnetic fields, and stellar wind. The variability of ξ^1 CMa (alias HD 46328, HR 2387, HIP 31125) is known for more than 100 years [23]. The period of its radial velocity variations was established 60 years ago as P=0.2096 d [24]. The range of radial velocity is $\Delta v_{\mathrm{rad}} = 34.2 \pm 0.7$ km s^{-1} [25]. ξ^1 CMa is one of the rare β Cep variables where the velocity amplitude exceeds the local speed of sound [26].

Together with the radial velocity variations, the star shows periodic photometric variability in visual light with a full amplitude of $\Delta m_{\mathrm{V}} = 0.034$ mag ($\approx$3.2%) [27]. Maximum light occurs about 25 min after minimum radius [25]. The amplitude of photometric variability increases strongly with decreasing wavelength; in the UV near $\lambda 1550$ Å it amounts to 0.161 mag [28].

ξ^1 CMa shows remarkable stability of its pulsational behavior: its period is constant to about 1 s century^{-1} [25]. The pulsations are non-linear and mono-periodic, with only one frequency and its first harmonic being significant [29, 26].

While there is good knowledge of the pulsation properties of ξ^1 CMa, its rotational velocity became established at $v \sin i = 10 \pm 2$ km s^{-1} only recently [22]. This value is consistent with

$v \sin i = 9 \pm 2 \, \text{km s}^{-1}$ derived independently from fitting high-resolution spectra by means of non-local thermodynamic equilibrium (NLTE) models [30].

The fundamental stellar parameters of ξ^1 CMa are typical for its spectral type B0.5IV [31]. The stellar effective temperature changes by $\Delta T_{\text{eff}} = 1000 \, \text{K}$ over the pulsation cycle, ranging from 27 000 K to 28 000 K, while $\log g$ changes between 3.7 at maximum and 3.8 at minimum [32, 22].

The chemical abundances in a sample of β Cep-type variables were derived from optical spectra using a NLTE line formation code and line blanketed LTE models, but neglecting stellar winds [22]. It was found that, similar to some other magnetic early B-type stars, nitrogen is overabundant by a factor of 3–4 in ξ^1 CMa as compared to the solar value.

The advent of UV spectroscopy provided evidence for a stellar wind from ξ^1 CMa [33]. The study of variability in its UV spectra obtained with the IUE observatory did not reveal temporal modulations [34].

The stellar wind parameters of ξ^1 CMa were constrained from the analysis of UV spectral lines by means of NLTE iron-blanketed model atmospheres calculated with the PoWR code [35]. The wind from ξ^1 CMa is weak, with a mass-loss rate of $\dot{M} < 10^{-10} \, M_\odot \, \text{yr}^{-1}$ and a terminal velocity of $v_\infty \sim 700 \, \text{km s}^{-1}$ [36].

The atmosphere models for ξ^1 CMa show that X-rays have a strong effect on the ionization of the stellar wind. The observed N V resonance doublet can be reproduced only by wind models that include X-rays. Interestingly, the emission measure (a density squared weighted volume) of the hot X-ray emitting plasma in ξ^1 CMa is significantly higher than that of the cool gas. Similar conclusions were reached for other late O and early B-type stars on the main sequence [37].

Despite earlier attempts [38], the first firm detection of a magnetic field on ξ^1 CMa was achieved only recently [39]. Periodic modulations of the longitudinal magnetic field with a

period of $\approx 2.2\,$d are observed. This period is identified with the stellar rotation. Using the known value of $v \sin i$ [22, 30], one can derive the inclination as $i \approx 3°$. The spectropolarimetric observations are best explained by assuming that our view of the rotation axis is almost pole-on while the magnetic axis is inclined by about $79°$ to the rotation axis; consequently, we have a nearly constant edge-on view of the system's magnetic equator (see Fig. 1). The field has a dipole geometry, albeit additional magnetic structures on smaller spatial scales cannot be excluded [10]. A summary of stellar parameters for ξ^1 CMa is provided in Table 1. Among pulsating B-type stars with known magnetic field, ξ^1 CMa has by far the strongest field with a polar strength of $\sim 5\,$kG [39].

While the magnetic field of ξ^1 CMa is strong, its stellar wind is relatively weak. Therefore, only at distances of more than $20\,R_*$ the stellar wind can enforce the magnetic field lines to become approximately radial. Below this distance, the stellar wind is controlled by the magnetic field [36].

In this work we analyze new, sensitive X-ray observations of ξ^1 CMa. The first X-ray survey of β Cep-type stars was performed by the *Einstein* observatory [40]. ξ^1 CMa was detected as the most X-ray luminous star in this survey [40, 41]. First X-ray spectra were obtained with the *Rosat* observatory. It was found that the X-ray spectrum of ξ^1 CMa is somewhat harder than of other B-type stars [42]. Interestingly, during a 0.56 h exposure with *Rosat*, variability at the level of 25% was noticed, but attributed to spacecraft wobble [42].

2 Results

The X-ray data for ξ^1 CMa discussed in this paper were taken with the X-Ray Multi-Mirror Satellite XMM-Newton of the European Space Agency ESA. Its three telescopes illuminate five different instruments which always operate simultaneously and independently: RGS1 and RGS2 are Reflection Grating Spectrometers [43], achieving a spectral resolution of $\sim 0.07\,$Å
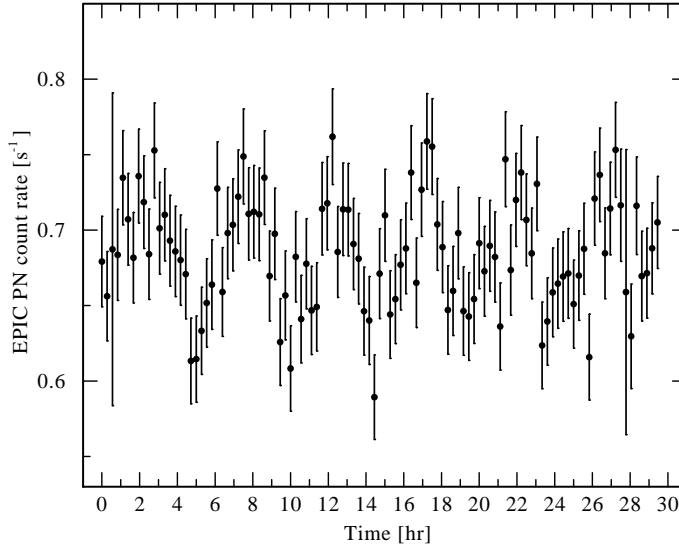
Figure 2: X-ray light curve of ξ^1 CMa in the $0.2\,\mathrm{keV} - 10.0\,\mathrm{keV}$ ($1.24\,\text{Å} - 62\,\text{Å}$) energy band where the background was subtracted. The horizontal axis denotes the time after the beginning of the observation in hours. The data were binned to $1000\,\mathrm{s}$. The vertical axis shows the count rate as measured by the EPIC PN camera. The error bars (1σ) correspond to the combination of the error in the source counts and the background counts.

in the wavelength range $5\,\text{Å} - 38\,\text{Å}$. The other three focal instruments, forming together the EPIC camera, are called MOS1 and MOS2 (Metal-Oxide Semiconductor) and PN (pn-CCDs). Compared to the RGSs, the EPIC instruments have a broader wavelength coverage of $1.2\,\text{Å} - 60\,\text{Å}$, but their spectral resolution is much lower ($E/\Delta E \approx 20 - 50$) [44, 45].

The first dedicated XMM-Newton observation of ξ^1 CMa started on 2009-09-03 with an exposure time of $2\,\mathrm{h}$, which was far too short to reveal the periodic variability [36]. In October 2012, XMM-Newton continuously observed ξ^1 CMa during nearly 29 hours. The light curves and spectra were recorded by all instruments. The sensitivity of the PN camera is superior, and therefore its data are best suited for time variability studies.

The data reduction involved standard procedures of the XMM-Newton Science Analysis System (SAS) v.13.0.1. The event lists have been filtered, and time intervals affected by high background were excluded. The useful exposure time was about $29\,\mathrm{h}$. The object of our study

7

is sufficiently isolated, with no nearby bright optical or X-ray sources.

The visual magnitude of ξ^1 CMa is $m_V = 4.33$ mag with a pulsation amplitude of 0.034 mag [1]. Because of the brightness of the target in the visual, the optical light blocking filter of XMM-Newton was used in its "thick" mode for our observations. We carefully investigated the potential contamination of the signal by optical/UV light. For the XMM-Newton detectors operating in full-frame mode and with the thick filter, no optical loading is expected for stars with $m_V > 0$ mag (XMM-Newton User Handbook). Moreover, the optical loading would affect the softest part of the X-ray spectrum only, but we don't see different pulsational behavior between softer and harder parts. Also, while optical pulsations have an amplitude of about 3%, the amplitude of X-ray pulsations is 10%. From these considerations, a contamination of the signal by optical/UV light can be ruled out.

2.1 X-ray light curve and comparison with optical light curve

Visual inspection of the X-ray light curve already reveals the periodic variability (see Fig. 2). To quantify this variability, a statistical analysis is performed. To obtain a characterization of the variability, the light curves in three energy bands ("total": 0.2 keV–10.0 keV ($1.24\,\text{Å} - 62\,\text{Å}$); "soft": 0.2 keV–1.0 keV ($12.4\,\text{Å} - 62\,\text{Å}$); and "hard": 1.0 keV–10.0 keV ($1.24\,\text{Å} - 12.4\,\text{Å}$)) are extracted from the event lists of all three EPIC instruments separately. This is done using the SAS's task EPICLCCORR, which provides equivalent on-axis, full point spread function count rates with background correction. The data are binned in temporal bins of different duration (100 s, 500 s, 1000 s, 3600 s).

For the further analysis, we first employ a χ^2 test for several hypotheses such as constancy, linear variation, and quadratic variation [46]. The PN and MOS1 data in soft and total bands display significant variations for all time binnings – the probability that the observed curve occurs by chance is < 0.01. Second, an autocorrelation test is performed to search for recurrence.

Variability on a timescale of about five hours is detected in PN and MOS1, but is not obvious in the MOS2 data due to its poorer sensitivity.

Finally, a Fourier algorithm is applied [47, 48], which detects a period of 4.87 ± 0.09 h in the PN data. This is much shorter than the plausible rotation period of the star, but is conspicuously similar to the stellar pulsation period as derived from optical photometry (5.03 h).

Simultaneous optical and X-ray observations of ξ^1 CMa are not available. In order to investigate the phase correlation between X-ray and optical pulsations, we searched for optical photometric data in the archives. The best and most recent photometry of ξ^1 CMa was obtained by the space telescope *Hipparcos* during the years 1990 - 1993. The *Hipparcos* photometry was carried out in a wide pass-band, referred to as $H_{\rm p}$ [49]. All $H_{\rm p}$ photometric data were analyzed in a uniform and self-consistent manner and yielded the parameters of variability which are compiled in the "*Hipparcos* Catalogue Epoch Photometry Data". The median magnitude of ξ^1 CMa is $H_{\rm p} = 4.2586$ mag, and the full variability amplitude is 0.0398 mag. Based on the 5482 observed cycles, the derived period is $P = 0.209577 \pm 0.000001$ d and the epoch of zero phase is JD(TT) 2448500.0280. We retrieved the *Hipparcos* photometric data for ξ^1 CMa and folded them according to the *Hipparcos* ephemeris. The result is shown in Figure 3 (lower panel). Comparing this ephemeris to older measurements from 1954 [27], the light curve is found to be still in phase, i.e. the period derived from *Hipparcos* photometry is very precise and the pulsations have been stable over 40 years.

Our *XMM-Newton* data were obtained about 34000 pulsation cycles after the *Hipparcos* measurements. However, given the stability of the ξ^1 CMa light curve [25], the *Hipparcos* ephemeris can be meaningfully applied for the epoch of our X-ray observations. The X-ray light curves were phased with the *Hipparcos* ephemeris and compared to the optical ones. Figure 3 shows the comparison between X-ray light curves in full, hard, and soft bands and the *Hipparcos* optical light curve. The X-ray light curve in broad band as well as in softer and harder bands
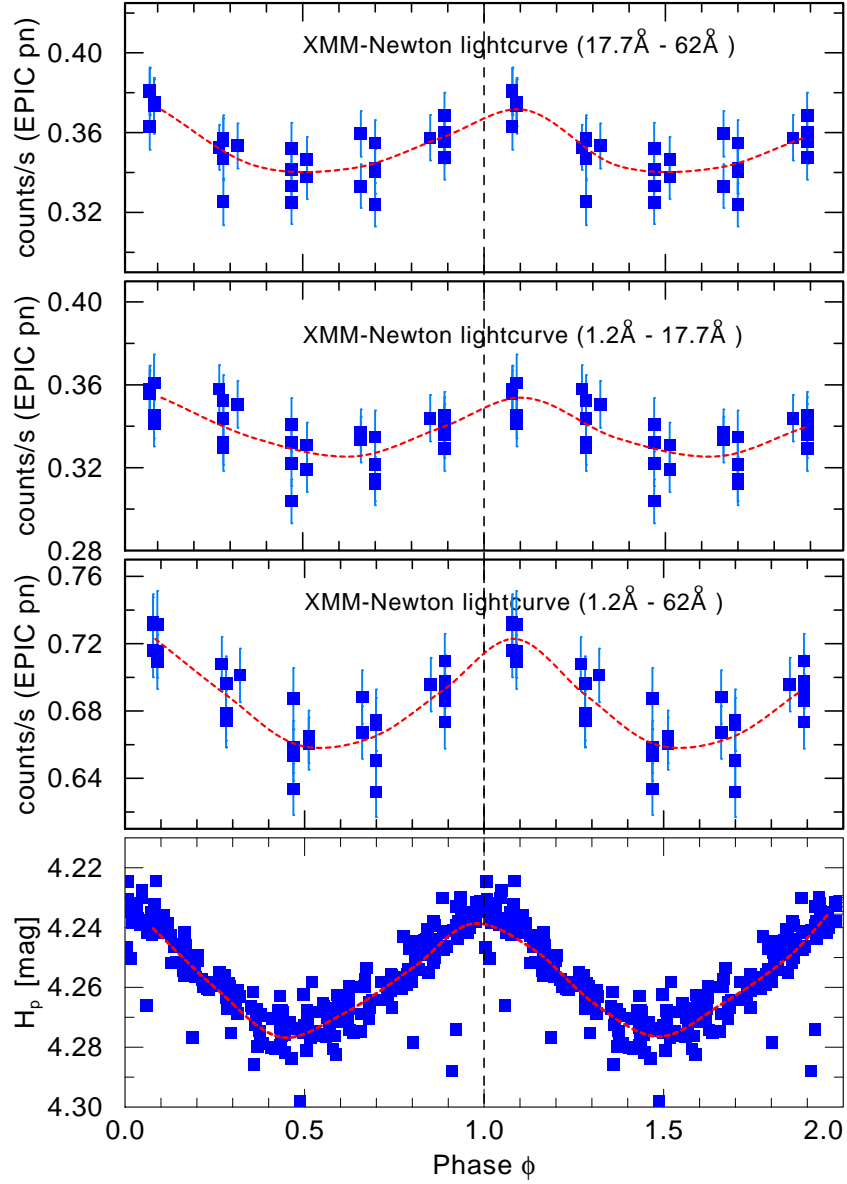
Figure 3: X-ray (three upper panels) and optical (lowest panel) light curves of ξ^1 CMa, phased with the stellar pulsation period. The X-ray light curve is produced from the data obtained with the *XMM-Newton* EPIC PN camera, using 1 h binning. The X-ray data are background subtracted, and the error bars (1σ) reflect the combination of the statistical errors in the source counts and the background. The dashed red line interpolates the averages in phase bins of $\Delta\phi = 0.1$. The lower panel shows the *Hipparcos* Catalogue Epoch Photometry data. The abscissa is the magnitude $H_{\rm p}$ in the *Hipparcos* photometric system (330-900 nm with maximum at ≈ 420 nm). The dashed red line interpolates the averages.

turned out to be in phase with the optical within the precision of the measurement and the formal error margin of the ephemeris (see Fig. 3).

Typically, the optical light curve of β Cep-type variables is similar in shape to the radial-velocity curve but lags in phase. The maximum brightness occurs shortly after the stellar radius goes through its minimum. The results of our analysis show that the same is true for the X-ray light – the maximum X-ray brightness is observed close to the phase when the stellar radius is at its minimum.

2.2   Analysis of the low-resolution X-ray spectra

To define the physical properties of the X-ray emitting plasma in ξ^1 CMa, we analyze its X-ray spectra. As a first step, the low resolution data recorded by the EPIC cameras [44, 45] are considered. While individual lines, in general, cannot be resolved with the EPIC, the low-resolution spectra cover a broad energy band and allow to constrain the temperature and the emission measure of the hot plasma. For a phase-resolved analysis, the spectra are extracted for time intervals close to the pulsation maximum (see Fig. 4) and the pulsation minimum, respectively.

The spectra are analyzed with the standard spectral fitting software XSPEC [50]. In order to reduce the number of free model parameters, the interstellar (ISM) neutral hydrogen column density is fixed at $N_{\mathrm{H}} = 1.4 \times 10^{20}\,\mathrm{cm}^{-2}$ according to the interstellar reddening which we obtained from fitting the observed spectral energy distribution from the UV to the optical [36], and in agreement with other works [51]. The fit of the X-ray spectra which we obtain with this hydrogen column density indicates that no additional absorption intrinsic to the source is required.

The spectra were investigated for the presence of an emission component described by a power law. Such emission is the dominant component in spectra of X-ray pulsars containing
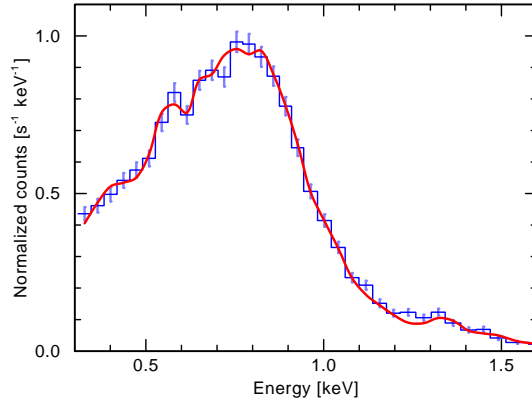
11

Figure 4: XMM-Newton PN spectrum of ξ^1 CMa at phases close to the maximum ($\phi = 0 \pm 0.15$). The observations are represented by the blue histogram with error bars corresponding to 3σ. The red curve shows the best fit model of a three-temperature plasma (see Table 2 for the parameters).

a neutron star. No convincing evidence for non-thermal radiation was found. Therefore, we adopt a model of thermal plasma in collisional ionization equilibrium as implemented in the APEC code [52]. To restrict the number of free parameters, we use only three temperature components. Albeit such a model provides only a simplified description of the plasma, it can give an insight in the characteristic temperatures and emission measures.

The abundances were set to solar values [53] for all elements included in the APEC model, except for nitrogen and oxygen, which were free fitting parameters. The best fit resulted in a nitrogen overabundance by a factor of 4.3 ± 0.8 relative to solar, and an oxygen overabundance by a factor of 1.6 ± 0.3. These abundances are in agreement with those found from the analysis of optical spectra of ξ^1 CMa [54].

The best fit to the observed spectra with a three-temperature plasma model is obtained with temperatures ranging between 1.2 and 9 million Kelvin (see Table 2). Spectral fits indicate that at the maximum of the pulsation cycle the plasma's mean temperature (i.e. the average temperature weighted with emission measure) is somewhat higher (by 500 000 K) than at minimum. During the pulsation cycle, the X-ray flux changes by $\approx 10\%$. From the time between max-

12

Table 2: X-ray spectral properties of ξ^1 CMa from fitting the low-resolution EPIC spectra at phases close to minimum and maximum

	minimum	maximum
kT_1 [keV]	0.110 ± 0.005	0.115 ± 0.006
EM_1 [10^{53} cm^{-3}]	9.66 ± 1.66	8.48 ± 1.38
kT_2 [keV]	0.32 ± 0.02	0.33 ± 0.02
EM_2 [10^{53} cm^{-3}]	6.37 ± 0.91	5.71 ± 0.79
kT_3 [keV]	0.80 ± 0.02	0.77 ± 0.02
EM_3 [10^{53} cm^{-3}]	3.96 ± 0.30	4.62 ± 0.30
$\langle kT \rangle \equiv \sum_i kT_i \cdot \mathrm{EM}_i / \sum_i \mathrm{EM}_i$ [keV]	0.31	0.34
F_X [erg s^{-1} cm^2]	1.04×10^{-12}	1.15×10^{-12}

imum and minimum of the light curve (2.5 h) one can estimate the cooling rate and use it to constrain the density of X-ray emitting plasma. We computed cooling functions with the APEC code, and found that the observed cooling rate can only be achieved if the electron density is higher than $\approx 3 \times 10^8$ cm^{-3}.

According to our PoWR models for the cool wind of ξ^1 CMa, such high electron densities are encountered only close to the photospheric radius R_*, and not farther than $1.05\,R_*$. Assuming that the electron densities of the hot X-ray emitting plasma are not higher than the densities of the ambient cool wind, the pulsed X-ray emission should originate from regions very close to the stellar photosphere.

2.3   Analysis of the high-resolution X-ray spectrum

The high-resolution X-ray spectra of ξ^1 CMa obtained with the RGS1 and RGS2 spectrographs [43] are dominated by strong emission lines of metals (see Fig. 5).

X-ray line profiles formed in a rapidly expanding stellar wind would be Doppler broadened. These lines can appear characteristically blue-shifted and asymmetric, especially when there is significant absorption of the X-rays in the cool stellar wind [7, 8]. To estimate the effects of
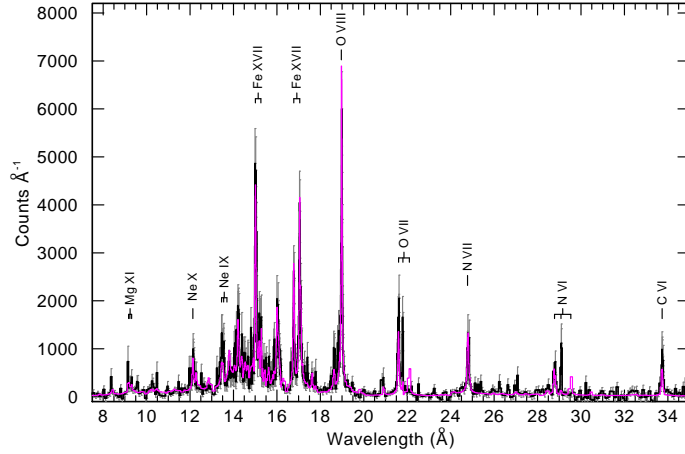
Figure 5: Combined RGS1+2 spectrum of ξ^1 CMa (black line) with the best fit model (red line). The spectrum is integrated over the full exposure time (25.9 h). Strong emission lines are identified.

wind absorption, we computed the radii at which the wind becomes optically thin for X-rays. As can be seen from Fig. 6, the wind of ξ^1 CMa is optically thin for X-rays above $1.01\,R_*$. Hence no significant effects of wind absorption are expected.

To analyze the line shape, both RGS spectra were combined and line moments were calculated. Because of high signal-to-noise ratio, the best-suited line for a detailed analysis is O VIII Lyα. This line is marginally broader than the instrumental response. The maximum wind velocity in ξ^1 CMa is $\approx 700\,\mathrm{km\,s^{-1}}$. If X-ray lines were formed in a plasma moving with such velocity, the corresponding Doppler line broadening would be detectable in the high-resolution spectrum. Only for the O VIII Lyα line a marginal blue-shift is detected, while the other line are inconclusive. Hence the emitting plasma is not moving rapidly, and the attenuation of the X-rays by the cool wind is low.

The spectrum obtained over the total exposure time and thus covering different pulsation phases can be well modeled by a thermal, optically thin plasma with temperatures that are consistent with those found from fitting the low-resolution spectra as described above (see Fig. 5).

As a next step, we considered how the high-resolution spectrum varies between different
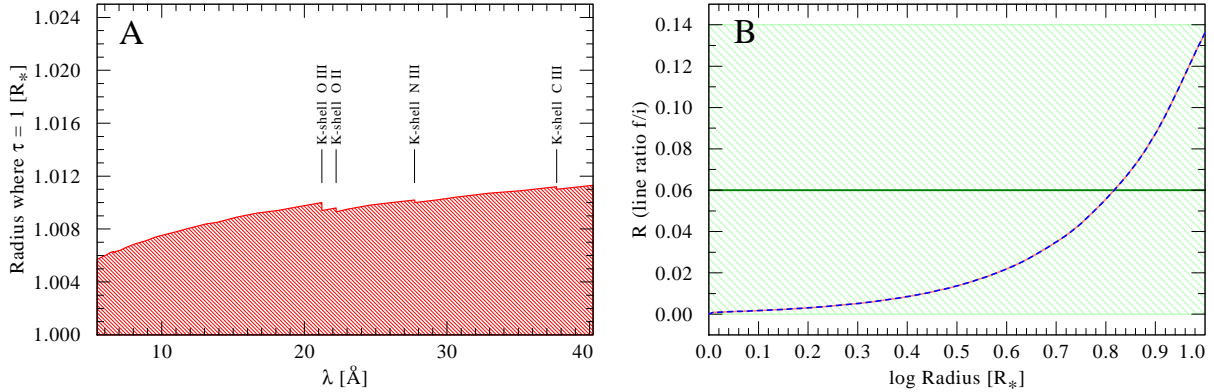
14

Figure 6: *Left panel:* Radius (in units of the stellar radius R_*) where the cool wind from ξ^1 CMa becomes optically thin in dependence on the wavelength. The calculations were performed with the PoWR stellar atmosphere code (see text) with stellar parameters from Table 1. The prominent photoionization edges are identified. *Right panel:* Dependence of the line ratio $R = f/i$ for the O VII lines as function of the radial location of the emitting plasma. Based on the PoWR model, the red curve accounts only for radiative de-population, while the almost identical blue curve also includes collisional processes under the assumption that the shocked plasma has the same density as the cool wind. The measured value is shown as horizontal green line, with the green hatched area representing the 1σ confidence band of the measurement.

pulsation phases (see Fig. 7). While the spectrum close to minimum light can be well reproduced with a three-temperature plasma model, there are difficulties in finding a suitable model that fits the high-resolution spectrum at maximum. Surprisingly, the line ratios between the CNO elements are different in different pulsation phases. Especially interesting is the variability of the N VII Lyα resonance line. This line is much stronger at the maximum than at the minimum of the light curve (see Table 3). We tried to reproduce this line variability by selecting models with different temperatures or additional absorption components, but could not find a convincing explanation for the observed line variability. Allowing the nitrogen abundance to be a free fitting parameter results in a lower nitrogen abundance during the phase close to the minimum (4 ± 1 solar nitrogen abundance in maximum versus 2 ± 1 in minimum). This is a puzzling result.

The location of X-ray emitting plasma can be constrained with the help of the lines from

Table 3: Photon flux in the N VII $\lambda 24.78$ Å line at different pulsation phase

Pulsation phase	Photon flux [cm^{-2}s^{-1}]
Average	$(2.6 \pm 0.4) \times 10^{-5}$
Maximum ($\phi = -0.9 - 0.2$)	$(3.6 \pm 0.7) \times 10^{-5}$
Middle ($\phi = 0.75 - 0.9$)	$(2.3 \pm 0.5) \times 10^{-5}$
Minimum ($\phi = 0.4 - 0.75$)	$(1.3 \pm 0.6) \times 10^{-5}$

helium-like ions. These ions emit a group of three X-ray lines, consisting of a forbidden (f), an intercombination (i), and a resonance (r) transition – the so-called fir triplet. The ratio of fluxes $G = (f + i)/r$ is sensitive to the temperature, while the ratio of fluxes between the forbidden and the intercombination component, $R = f/i$, is sensitive to the electron density and the ultraviolet radiation field [55]:

$$R(r) = \frac{\mathcal{R}_0}{1 + \phi(r)/\phi_{\mathrm{c}} + N_{\mathrm{e}}(r)/N_{\mathrm{c}}}. \tag{1}$$

Here, ϕ denotes the photo-excitation rate from the term 2s ^{3}S to 2p^{3}P, and N_{e} is the electron density. The constants $\mathcal{R}_0, \phi_{\mathrm{c}}$, and N_{c} depend on atomic parameters and slightly on the electron temperature [55, 56]. Most important, the photo-excitation rate $\phi(r)$ scales with the mean intensity of the radiation field at the wavelength of the $f \to r$ transition, which is typically in the UV.

The fir triplets of Ne IX, O VII, and N VI are present in the RGS spectrum of ξ^1 CMa, with the O VII triplet being the strongest one. Only in the O VII triplet, the forbidden line is marginally detected, while forbidden lines in Ne IX and N VI were not detected.

We use the PoWR stellar atmosphere model to calculate the values of $R(r)$ for Ne IX, O VII and N VI as function of the radial location in the wind of ξ^1 CMa. The photo-excitation rates $\phi(r)$ are computed at each radius from the radiation intensity as provided by the PoWR model, which accounts not only for geometric dilution, but also for the diffuse radiation field. Figure 6
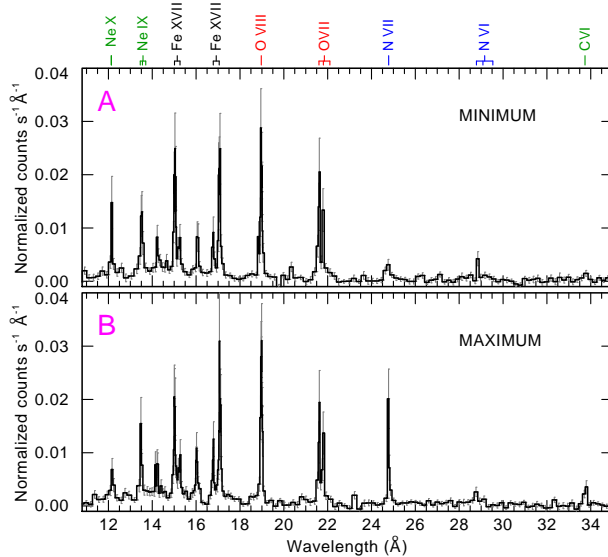
Figure 7: Combined high-resolution (RGS1+RGS2) X-ray spectra of ξ^1 CMa in phases close to the pulsation minimum (upper panel, $\phi = 0.5 \pm 0.17$) and pulsation maximum (lower panel, $\phi = 0 \pm 0.15$), respectively. Strong emission lines are identified. The error bars correspond to 3σ.

(right panel) shows for the O VII triplet the predicted R ratio as function of the radial location of the emitting plasma. From the spectrum integrated over the full exposure time, the best-fit value of the R ratio indicates a plasma location at $\approx 6\,R_*$, while the 1σ margins are consistent with any location between $1\,R_*$ and $10\,R_*$.

3 Discussion

It is generally assumed that X-ray emission from hot massive stars originates from plasma heated by hydrodynamic shocks in a radiatively driven stellar wind. The radiation driven wind theory predicts that the mass loss rate depends on the stellar parameters as

$$\dot{M} \propto L_{\mathrm{bol}}^{\frac{1}{\alpha}} M_{\mathrm{eff}}^{\frac{\alpha-1}{\alpha}}, \tag{2}$$

where L_{bol} is the stellar bolometric luminosity and α is a dimensionless number (which is about 2/3) representing the power-law exponent of the distribution function of line strength of the

thousands of spectral lines driving the wind, and $M_{\text{eff}} \approx M_*$ for B-type stars [57, 58].

During a pulsation cycle, the radius of ξ^1 CMa changes by 4% and its effective temperature changes by 3.6%, with consequent changes for the luminosity. Recall that the luminosity is given by $L_{\text{bol}} = 4\pi R_*^2 \sigma T_{\text{eff}}^4$, where σ is Stefan–Boltzmann constant. With R_* and T_{eff} varying in anti-phase, the bolometric luminosity changes by $\approx 7\%$ during a pulsation cycle. According to equation (2), the mass-loss rate may change by 10%, which is a similar amplitude as of the observed X-ray pulsations. According to the wind theory, the wind velocity scales with the escape velocity, i.e. proportional to $\sqrt{M_{\text{eff}} R_*^{-1}}$. Therefore it may also slightly change during the pulsation. The dynamical time scale for a stellar wind is the flow time $R_* v_\infty^{-1}$. For ξ^1 CMa this time is about 2 h. Hence, the wind is principally able to follow changes that are triggered with the pulsation period (5 h). From these considerations one might, in principle, expect that the stellar pulsations lead to periodic changes of the wind parameters and, consequently, of the X-ray luminosity. It is interesting to note that there is an established empirical correlation between bolometric and X-ray luminosity for OB type stars, $L_{\text{X}} \sim 10^{-7} L_{\text{bol}}$ [59].

However, while these scaling correlations are general, no X-ray pulsations from other stars were detected so far. For instance, a dedicated study of the X-ray light curve of β Cephei obtained with XMM-Newton did not reveal the presence of pulsations [60]. We, therefore, believe that the general scaling correlations do not explain the observed X-ray properties of ξ^1 CMa.

The new XMM-Newton observations of ξ^1 CMa may provide important insights into possible mechanisms of plasma heating. In massive stars that possess large scale magnetic fields, plasma heating is commonly explained by the magnetically confined wind shock mechanism (MCWS) [15, 16]. This model predicts that the parameters of X-ray emission depend on mass-loss rate, wind velocity, stellar rotation, and especially on the magnetic field strength [61, 62].

To check these predictions, we compared our data with RGS spectra of comparable quality

that are available for two other magnetic β Cep-type stars, β Cen (B1III) and β Cep (B2V). β Centauri is a binary system consisting of two β Cep-type stars of nearly equal mass [63]. The primary rotates significantly faster ($v\sin i = 190 \pm 20\,\mathrm{km\,s^{-1}}$) than the magnetic secondary ($v\sin i = 75 \pm 15\,\mathrm{km\,s^{-1}}$) [63, 64]. For its spectral class, β Centauri has an average X-ray luminosity, $L_{\mathrm{X}} = 1 \times 10^{31}\,\mathrm{erg\,s^{-1}}$. From the analysis of its X-ray spectrum, the temperature of the X-ray emitting plasma is $\langle kT \rangle \approx 0.3\,\mathrm{keV}$, similar to the one measured in ξ^1 CMa. The ratios of forbidden to intercombination line strengths in He-like ions are also similar to those in ξ^1 CMa [65].

β Cephei is also a binary system, which consists of a magnetic B1V star as primary [66] and secondary of type B6-8e [67]. The temperature of the X-ray emitting plasma is also $\langle kT \rangle \approx 0.3\,\mathrm{keV}$, is similar to ξ^1 CMa [60]. The forbidden to intercombination line ratio in He-like ions is basically identical with those measured in ξ^1 CMa.

The wind parameters are also quite similar in β Cen, β Cep and ξ^1 CMa. However the magnetic field strength of ξ^1 CMa is at least one order of magnitude higher than in other two objects. Moreover, the viewing geometry of ξ^1 CMa may be special as we likely look face on at the plane of the stellar rotational equator. Yet, the X-ray temperatures and the locations of hot plasma are similar in all three stars.

Besides MCWSs, another possibility for plasma heating in β Cep-type variables could be the deposition of mechanical energy from the stellar pulsations [68, 69]. However, in a study of a small sample of β Cep-type variables, no dependence of the X-ray luminosity on the pulsational period or amplitude was noticed [36].

The properties that make ξ^1 CMa distinct from other β Cep-type variables are the supersonic speed of the pulsating photosphere, the high strength of the star's magnetic field, and the absence of non-radial modes in the stellar oscillations. We suggest that a successful explanatory model must take these ingredients into account in order to understand the X-ray emission and

its periodic modulations observed in ξ^1 CMa.

To summarize, we detect pulsations of the X-ray flux from ξ^1 CMa in phase with optical pulsations but with larger amplitude. The X-ray light curves are similar in different energy bands. There are tentative indications that changes of the X-ray emission are due to the plasma heating and cooling – from the spectral analysis, somewhat higher temperatures are deduced at X-ray maximum as compared to X-ray minimum. The X-ray emitting plasma is located close to the photosphere, as follows from the cooling rate and from the analysis of line ratios in He-like ions.

This first discovery of X-ray pulsations from a non-degenerate, massive stars will stimulate theoretical considerations for the physical processes operating in magnetized stellar winds. So far, the mechanism by which the X-rays are affected by the stellar pulsation remains enigmatic.

References and Notes

[1] A. Stankov, G. Handler, *ApJS* **158**, 193 (2005).

[2] W. A. Dziembowski, A. A. Pamiatnykh, *MNRAS* **262**, 204 (1993).

[3] A. Heger, C. L. Fryer, S. E. Woosley, N. Langer, D. H. Hartmann, *ApJ* **591**, 288 (2003).

[4] L. B. Lucy, P. M. Solomon, *ApJ* **159**, 879 (1970).

[5] A. Feldmeier, R. Kudritzki, R. Palsa, A. W. A. Pauldrach, J. Puls, *A&A* **320**, 899 (1997).

[6] W. L. Waldron, J. P. Cassinelli, *ApJ* **668**, 456 (2007).

[7] J. J. Macfarlane, *et al.*, *ApJ* **380**, 564 (1991).

[8] R. Ignace, *ApJ* **549**, L119 (2001).

[9] L. M. Oskinova, A. Feldmeier, W.-R. Hamann, *MNRAS* **372**, 313 (2006).

[10] S. Hubrig, *et al.*, *ApJ* **726**, L5 (2011).

[11] S. Hubrig, *et al.*, *A&A* **528**, A151 (2011).

[12] Grunhut, J. H., Wade, G. A., and MiMeS Collaboration. The Incidence of Magnetic Fields in Massive Stars: An Overview of the MiMeS Survey Component. *AIP Conf. Proc.* **1429**, 67–74, (2012).

[13] L. Ferrario, J. E. Pringle, C. A. Tout, D. T. Wickramasinghe, *MNRAS* **400**, L71 (2009).

[14] J. Braithwaite, *ArXiv e-prints* (2013).

[15] J. Babel, T. Montmerle, *ApJ* **485**, L29+ (1997).

[16] A. ud-Doula, S. P. Owocki, *ApJ* **576**, 413 (2002).

[17] L. M. Oskinova, D. Clarke, A. M. T. Pollock, *A&A* **378**, L21 (2001).

[18] Y. Nazé, *et al.*, *A&A* **520**, A59+ (2010).

[19] J. Donati, *et al.*, *MNRAS* **326**, 1265 (2001).

[20] R. Ignace, *et al.*, *ApJ* **775**, 29 (2013).

[21] M. Güdel, Y. Nazé, *A&A Rev.* **17**, 309 (2009).

[22] T. Morel, K. Butler, C. Aerts, C. Neiner, M. Briquet, *A&A* **457**, 651 (2006).

[23] E. B. Frost, *ApJ* **25**, 59 (1907).

[24] D. H. McNamara, *PASP* **65**, 193 (1953).

[25] R. R. Shobbrook, *MNRAS* **162**, 25 (1973).

[26] S. Saesen, M. Briquet, C. Aerts, *Communications in Asteroseismology* **147**, 109 (2006).

[27] A. D. Williams, *PASP* **66**, 200 (1954).

[28] J. R. Lesh, P. R. Wesselius, *A&A* **79**, 115 (1979).

[29] D. Heynderickx, C. Waelkens, P. Smeyers, *A&AS* **105**, 447 (1994).

[30] K. Lefever, *et al.*, *A&A* **515**, A74 (2010).

[31] D. R. Gies, D. L. Lambert, *ApJ* **387**, 673 (1992).

[32] A. van Hoof, *ZAp* **56**, 141 (1963).

[33] G. J. Peters, *PASP* **85**, 536 (1973).

[34] R. S. Schnerr, *et al.*, *A&A* **483**, 857 (2008).

[35] W. Hamann, G. Gräfener, *A&A* **427**, 697 (2004).

[36] L. M. Oskinova, *et al.*, *MNRAS* **416**, 1456 (2011).

[37] D. P. Huenemoerder, *et al.*, *ApJ* **756**, L34 (2012).

[38] R. J. Rudy, J. C. Kemp, *MNRAS* **183**, 595 (1978).

[39] S. Hubrig, *et al.*, *MNRAS* **369**, L61 (2006).

[40] P. C. Agrawal, K. P. Singh, G. R. Riegler, R. A. Stern, *MNRAS* **208**, 845 (1984).

[41] F. Grillo, S. Sciortino, G. Micela, G. S. Vaiana, F. R. Harnden, Jr., *ApJS* **81**, 795 (1992).

[42] J. P. Cassinelli, D. H. Cohen, J. J. Macfarlane, W. T. Sanders, B. Y. Welsh, *ApJ* **421**, 705 (1994).

[43] J. W. den Herder, *et al.*, *A&A* **365**, L7 (2001).

[44] M. J. L. Turner, *et al.*, *A&A* **365**, L27 (2001).

[45] L. Strüder, *et al.*, *A&A* **365**, L18 (2001).

[46] Y. Nazé, L. M. Oskinova, E. Gosset, *ApJ* **763**, 143 (2013).

[47] A. Heck, J. Manfroid, G. Mersch, *A&AS* **59**, 63 (1985).

[48] E. Gosset, P. Royer, G. Rauw, J. Manfroid, J.-M. Vreux, *MNRAS* **327**, 435 (2001).

[49] F. van Leeuwen, *et al.*, *A&A* **323**, L61 (1997).

[50] K. A. Arnaud, *Astronomical Data Analysis Software and Systems V*, G. H. Jacoby & J. Barnes, ed. (1996), vol. 101 of *Astronomical Society of the Pacific Conference Series*, p. 17.

[51] S. B. Gudennavar, S. G. Bubbly, K. Preethi, J. Murthy, *ApJS* **199**, 8 (2012).

[52] R. K. Smith, N. S. Brickhouse, D. A. Liedahl, J. C. Raymond, *ApJ* **556**, L91 (2001).

[53] M. Asplund, N. Grevesse, A. J. Sauval, P. Scott, *ARA&A* **47**, 481 (2009).

[54] T. Morel, S. Hubrig, M. Briquet, *A&A* **481**, 453 (2008).

[55] G. R. Blumenthal, G. W. F. Drake, W. H. Tucker, *ApJ* **172**, 205 (1972).

[56] D. Porquet, R. Mewe, J. Dubau, A. J. J. Raassen, J. S. Kaastra, *A&A* **376**, 1113 (2001).

[57] H. J. G. L. M. Lamers, J. P. Cassinelli, *Introduction to Stellar Winds* (1999).

[58] R. P. Kudritzki, *Stellar astrophysics for the local group: VIII Canary Islands Winter School of Astrophysics*, A. Aparicio, A. Herrero, F. Sánchez, eds. (1998), p. 149.

[59] R. Pallavicini, *et al.*, *ApJ* **248**, 279 (1981).

[60] F. Favata, C. Neiner, P. Testa, G. Hussain, J. Sanz-Forcada, *A&A* **495**, 217 (2009).

[61] M. Maheswaran, J. P. Cassinelli, *MNRAS* **394**, 415 (2009).

[62] A. Ud-Doula, S. P. Owocki, R. H. D. Townsend, *MNRAS* **392**, 1022 (2009).

[63] M. Ausseloos, C. Aerts, K. Lefever, J. Davis, P. Harmanec, *A&A* **455**, 259 (2006).

[64] E. Alecian, *et al.*, *A&A* **536**, L6 (2011).

[65] A. J. J. Raassen, J. P. Cassinelli, N. A. Miller, R. Mewe, E. Tepedelenlioğlu, *A&A* **437**, 599 (2005).

[66] J. Donati, *et al.*, *MNRAS* **326**, 1265 (2001).

[67] R. S. Schnerr, H. F. Henrichs, R. D. Oudmaijer, J. H. Telting, *A&A* **459**, L21 (2006).

[68] J. P. Cassinelli, *et al.*, *ApJ* **460**, 949 (1996).

[69] H. R. Neilson, J. B. Lester, *ApJ* **684**, 569 (2008).